Resolution Considerations for Structured Illumination Microscale Particle Tracking Velocimetry

M. Spadaro[1], M. Yoda[1,*]

1: George W Woodruff School of Mechanical Engineering, Georgia Institute of Technology, United States of America

* Correspondent author: minami@gatech.edu

Keywords: Microfluidics, particle tracking velocimetry, optical diagnostics, structured illumination microscopy

ABSTRACT

In microscale particle velocimetry, the spatial resolution of velocity measurements along the optical axis is often degraded by signal from tracer particles outside the focal plane. Structured illumination microscopy particle tracking velocimetry (SIM PTV) can eliminate most of this out-of-focus signal by using illumination with a non-zero spatial frequency to preferentially illuminate the in-focus particles. Two such (raw) images can then be combined to eliminate the background signal and demodulate the image. The objective of this study was to quantify and optimize the spatial and temporal resolution of SIM PTV based upon Poiseuille flow in a microchannel at Reynolds numbers $Re \approx 0.02$. The axial spatial resolution, estimated for this known velocity profile from the standard deviation of the velocity measurements, is improved (*i.e.*, reduced) by at least a factor of 2 compared with the results for a uniformly illuminated flow. This axial spatial resolution, which is given by the point spread function of the imaging system, is in good agreement with theory. The spatial frequency of the illumination that optimizes the spatial resolution is a function of the scattering area of the tracer particles. Interestingly, increasing the number of raw images does not appear to improve the axial resolution. Finally, the temporal resolution of SIM PTV is estimated based upon both image and velocity acquisition times.

1. Introduction

Optical diagnostic methods are valuable nonintrusive tools for experimentally quantifying the internal flow through microchannels with characteristic cross-sectional dimensions of O(1-100 μm). Such flows are widely used in biomedical applications, where microfluidic devices are used as "labs on a chip" to perform tasks such as cell, DNA, and protein analysis (Yeo et al. 2011), as well as cell sorting (Shields et al. 2015; Gao and Chen 2008). Optical diagnostic methods are also used to study multiphase transport including particle and droplet dynamics (Li et al. 2020; Shang et al. 2017).

Perhaps the most common microscale optical diagnostic technique is microscale particle velocimetry, where a flow is seeded with tracer particles that are convected by the flow. The motion of the particles is recorded over time and used to estimate two, or all three, velocity components in a plane, or a volume, of the flow. Particle tracking velocimetry (PTV) and particle image velocimetry (PIV) measure the displacements of individual, and groups of, particles, respectively, over two exposures separated by a known time interval. (Adrian et al. 2011; Raffel et al. 2018). These basic techniques can be extended to indirectly record 3D velocity data using defocused particle images (Yoon and Kim 2006) or holograms of particle images (Grare et al. 2015). More recently, light field microscopy has been used to record accurate 3D-2C velocity measurements by making use of a microlens array to encode depth information into the image (Truscott et al. 2017).

A typical optical setup for 2D-2C particle velocimetry uses a laser light sheet with a thickness of at least 0.5 mm to illuminate a single plane of the flow, and images this plane along an optical axis normal to the plane (Adrian, 2005). This configuration, however, requires optical access to the flow from two orthogonal directions, which is impractical in many microchannels which have optical access along only one direction. Most optical techniques therefore use uniform volume illumination of the microchannel, where most, if not all, of the channel cross section is illuminated along (*vs.* normal to) the optical axis (Lee et al. 2009). The images of the flow obtained with this type of illumination include unwanted signal from particles outside the focal plane, greatly decreasing the signal to noise ratio (SNR) and degrading the axial spatial resolution of flow parameters obtained from such images (Yoda 2020). Confocal microscopy can be used to improve the axial spatial resolution (Klein et al. 2012), but at the cost of temporal resolution; the total acquisition time of 2D images with commercial confocal microscopy systems, which scan a pinhole over the plane, are typically O(10 ms).

The term super-resolution microscopy describes a family of imaging techniques that can theoretically exceed the Abbe diffraction limit (Sigal et al. 2018). The groundwork for these techniques was laid by Lukosz (1966), who described the way in which the degrees of freedom of an optical "message" could be "exchanged" while keeping the total "number of degrees of freedom" constant. Hence, the spatial resolution of an image can be improved by reducing object area, and/or temporal degrees of freedom, among other parameters. Structured illumination microscopy (SIM) is a super-resolution technique that "exchanges" (improves) spatial resolution with (reduced) object area in a single image by using illumination with a nonzero spatial frequency (Neil 1997). SIM therefore requires multiple (raw) images to capture the entire object area, with a (spatial) shift in the illumination pattern. This approach is also the basis of structured (laser) illumination planar imaging (SLIPI) where structured laser light sheet illumination is used to enhance the in-plane spatial resolution of macroscale multiphase flow visualizations (Mishra et al. 2017) and velocimetry in atomizing sprays with droplet velocities of 20 to 200 m/s (Kristensson and Berrocal 2018).

We have instead used SIM in microscale flows, specifically for SIM particle tracking velocimetry (SIM PTV), with the aim to enhance the out-of-plane, or axial, spatial resolution, in a microchannel flow illuminated over its cross section. Double-exposure SIM (Zhou et al. 2015) is used to reconstruct a single image of the particle tracers from two raw images obtained with sinusoidally modulated illumination with a phase shift of π between the pair of raw images. Reconstruction involves a Hilbert transform that removes the signal from beyond the focal plane, and initial results in Poiseuille flow demonstrated that the technique significantly reduced the range of measured velocities, corresponding to halving the optical section "thickness" (*i.e.*, of the slice of the flow imaged by SIM), compared with that for "standard" micro-PTV with unstructured (*i.e.*, uniform) illumination (Spadaro and Yoda 2020).

The objective of this subsequent study is to further quantify and optimize the spatial and temporal resolution of the technique using planar Poiseuille flows at $Re \leq 0.02$ (*vs.* $Re \approx 10^{-3}$ in Spadaro and Yoda 2020) and a maximum speed of 0.23 mm/s. The axial spatial resolution, and how it depends upon the illumination spatial frequency and tracer particle concentration are quantified. The temporal resolution of the technique is defined and discussed based upon the time scales for a single reconstructed image and to acquire enough velocity samples to obtain a statistically converged mean.

2. Methods

These experiments studied planar Poiseuille flow through a 30 mm (x) × 0.1 mm (y) × 4 mm (z) microchannel as shown in figure 1*a*. The microchannel consists of double-sided strip of polyimide tape (Kapton® PPTDE-1) "sandwiched" between two borosilicate glass microscope slides, with a 2 mm diameter inlet and outlet at the ends of the channel. The flow is seeded at volume fractions $0.1\% \le \varphi \le 0.35\%$ with two types of fluorescent polystyrene (PS) particles: 1) radius a = 1.6 μm (Polysciences 17147) particles with excitation/emission maxima of 441 nm/486 nm; and 2) a = 2.4 μm (Thermo Scientific G0500) particles with excitation/emission maxima at 468 nm/508 nm. The working fluid, which is density-matched to the particles (nominal density ρ = 1.05 g/cm^3), is a mixture of either: 1) 50 vol% double-distilled deionized (DDI) + 50 vol% heavy water (D_2O); or 2) 80 vol% DDI water + 20 vol% glycerin (VWR 470301 reagent grade). Unless stated otherwise, the results presented here are obtained with a = 1.6 μm particles at φ = 0.2%.

The flow is hydrostatically driven by a pressure gradient dp/dx = 66.4–202 Pa/m through 3.2 mm inner diameter (ID) Tygon tubing and 3.2 mm ID borosilicate glass tube attached to the channel inlet. The outlet is connected to a 30 mm length of 3.2 mm ID Tygon tubing. Both the inlet and outlet tubes are connected using silicone sealant (General Electric GE5100). The flow Reynolds number $Re = UH/\nu = 7.2\times10^{-3}$–$2.2\times10^{-2}$ based on channel depth H = 100 μm and centerline speed $U \le 230$ μm/s.

Structured illumination with a sinusoidally varying intensity at spatial frequencies $\nu < 0.13$ μm^{-1} is generated by a 7 W plasma lamp (Thorlabs HPLS345) modulated ("structured") by a digital micromirror device (DMD) (Texas Instruments DLP6500FYE). A magnification M = 50, numerical aperture NA = 0.5 (Leica 566036) and a M = 100, NA = 0.8 (Olympus LMPLFLN 100X) microscope objective are used to illuminate and image the flow, respectively. The fluorescence from the a = 1.6 μm and a = 2.4 μm particle tracers is isolated from the illumination with a wavelength λ = 440±10 nm bandpass filter (Thorlabs FB440-10) and a λ = 470±10 nm bandpass filter (Thorlabs FB470-10), respectively, and recorded by an intensified CCD camera (Princeton Instruments PI-MAX4:1024i). Flow velocities are obtained at y/H = –0.3, 0, 0.1, 0.2, 0.3 and 0.4 (Fig. 1*b*), using at least 10 (reconstructed) image pairs per location.

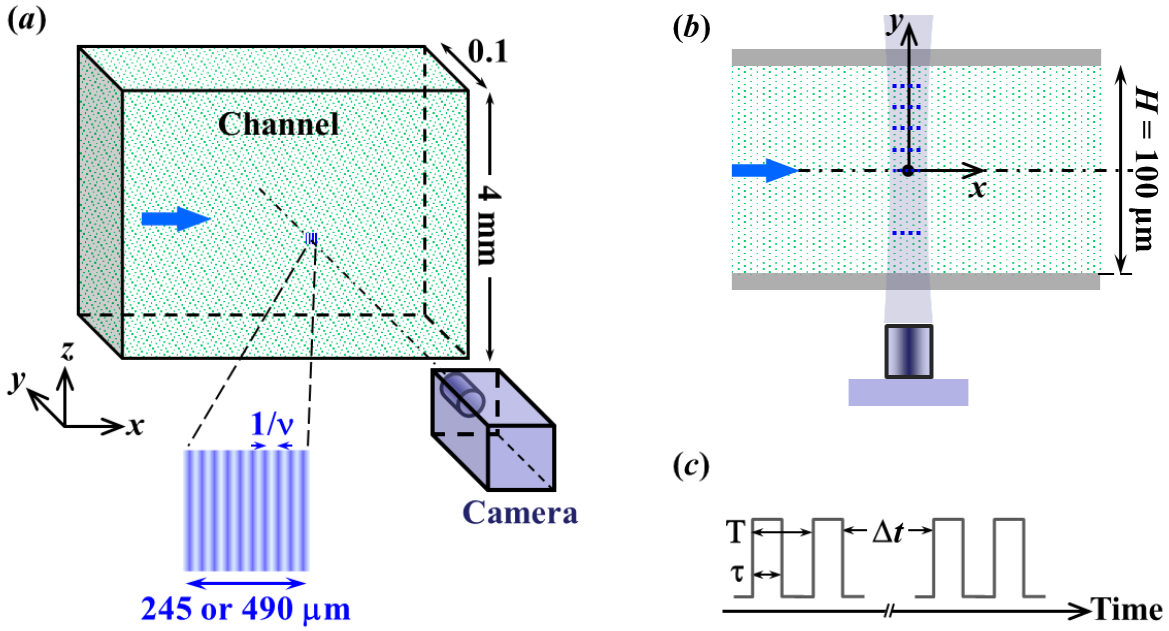

Fig. 1 (*a*) Sketch of experimental setup. (*b*) Flow locations for image acquisition. (*c*) Raw image acquisition timing diagram

A pair of raw images with a phase shift of π in the structured illumination and an exposure time τ = 1 ms were acquired with a period T = 2 ms, followed by the next pair of raw images starting Δt = 300 ms later (Fig. 1*c*). The total acquisition time for the two reconstructed images required to obtain velocity estimates was therefore T_p = 306 ms. Images were also obtained with uniform illumination for comparison purposes using the same illumination and imaging system with the DMD "off" under otherwise identical conditions. The region of the flow recorded in these images was either 245 μm or 490 μm square. Further details are given in Spadaro and Yoda (2020).

The raw images are first flat-field corrected, then Gaussian denoised using the MATLAB R2020a image processing toolbox. The second processed raw image in the pair is then subtracted from the first to remove the background. A complex image is constructed from this difference image and its Hilbert transform, and the magnitude of this complex image yields the reconstructed (and demodulated) image (Spadaro and Yoda 2020). Particles in the reconstructed image are detected using active contour mapping (Chan and Vese 2001), where particle images are taken to be connected groups of pixels above an adaptive local threshold determined using Otsu's method (Otsu 1979). The location of the particle center, defined here to be the grayscale-weighted center of the particle image, was determined with sub-pixel resolution. Particles are

tracked between reconstructed images to their nearest neighbors within a search window of 25% of the expected displacement between frames based on the known velocity field (*cf.* Eq. 1).

The reconstructed SIM PTV images in our previous work had anisotropic particle images, with particle images elongated along the z-direction, *i.e.*, the direction normal to the modulation. We found that this elongation was due to the presence of large imaginary components near the particles in the complex image. Thresholding the imaginary components within $3a$ of the center along the z-direction effectively eliminated the anisotropy in the reconstructed particle images. Note that this processing is solely for "aesthetic" purposes, since this anisotropy has no effect upon the location of the particle center, and hence little, if any effect on the particle velocities.

3. Results

Spatial Resolution

The spatial resolution along the optical axis, or axial spatial resolution, is defined here to be the "thickness" of the image reconstructed from two "raw" structured illumination images. For these particle velocimetry data, the axial spatial resolution is estimated from the velocities obtained from a pair of reconstructed images of Poiseuille flow with the known velocity field:

$$\frac{u}{U_c} = 1 - \left(\frac{2y}{H}\right)^2 \qquad \text{where } U_c = -\frac{H^2}{8\mu}\frac{dp}{dx} \qquad [1]$$

Here, u is the local velocity, U_c is the maximum velocity, which occurs at the channel centerline ($y = 0$), H is the channel width, μ is the fluid viscosity, and dp/dx is the applied pressure gradient.

Specifically, the axial spatial resolution δy is determined to be the range of y-values corresponding to the standard deviation σ_u in the velocity about the average velocity $\bar{u}$, so

$$\frac{\bar{u} - \sigma_u}{U_c} = 1 - \left[\frac{2y_F + (\delta y)}{H}\right]^2$$

or

$$\delta y = H\left(\sqrt{\frac{U_c - \bar{u} + \sigma_u}{U_c}}\right) - 2y_F \qquad [2]$$

where y_F is now the y-position of the focal plane. A smaller standard deviation therefore corresponds to a smaller, *i.e.*, improved, spatial resolution.

Figure 2 shows velocity profiles using structured (△) and uniform illumination (▲) in Poiseuille flow through a H = 100 μm channel at $Re = \rho U_c H/\mu$ = 0.021 (where ρ is the fluid density), corresponding to U_c = 0.23 mm/s. The spatial frequency of the illuminating light ν = 0.031 μm^{-1}. On average, σ_u for the SIM results is 40% those of the uniform illumination results, and the minimum δy = 15 μm for the SIM results, *vs.* 30 μm for the uniform illumination results. The axial resolution of SIM PTV is therefore half that for "standard" PTV, and a significant improvement over earlier results which reported an axial spatial resolution of 30 μm in Poiseuille flow at Re = 6.4×10^{-4}. Note that significant improvements in δy are only observed in the bulk flow at $|y/H| <$ 0.3 because the "structure", specifically the contrast, of the structured illumination, is degraded near the wall due to reflections of the illumination from the wall. These results also show that the values for $\bar{u}$ obtained with SIM PTV are in better agreement with the known velocity field in the bulk flow, with an average error of 1.6%, *vs.* an average error of 2.5% for the average velocities obtained with uniform illumination.

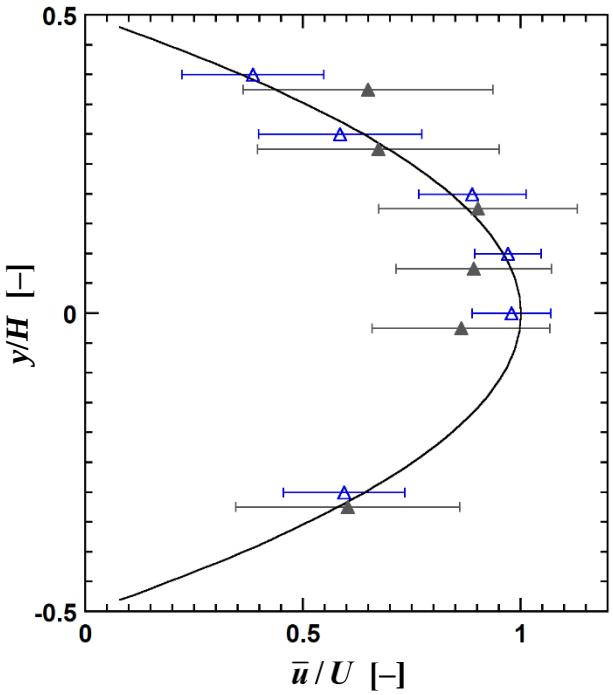

Fig. 2 Average particle velocities normalized by the centerline velocity $\bar{u}/U$ obtained using structured illumination (△) and uniform illumination (▲) in Poiseuille flow through a 100 μm deep channel at Re = 0.03. The velocity data are obtained at the same y/H, but have been offset vertically for visual clarity. The error bars represent the standard deviation in the velocities σ_u

The axial spatial resolution depends upon the spatial frequency of the sinusoidal illumination ν (Neil et al. 1997), which can be adjusted by modifying the DMD settings. Figure 3 shows δy estimated from Eq. [2] as a function of ν for particles of radius a = 1.6 μm (*blue symbols*) and 2.5 μm (*red symbols*) at particle volume fractions φ = 0.11% (◇), 0.2% (△) and 0.35% (○). In all cases, the minimum δy is achieved at the maximum value of ν; the smallest $\delta y \approx 14$ μm.

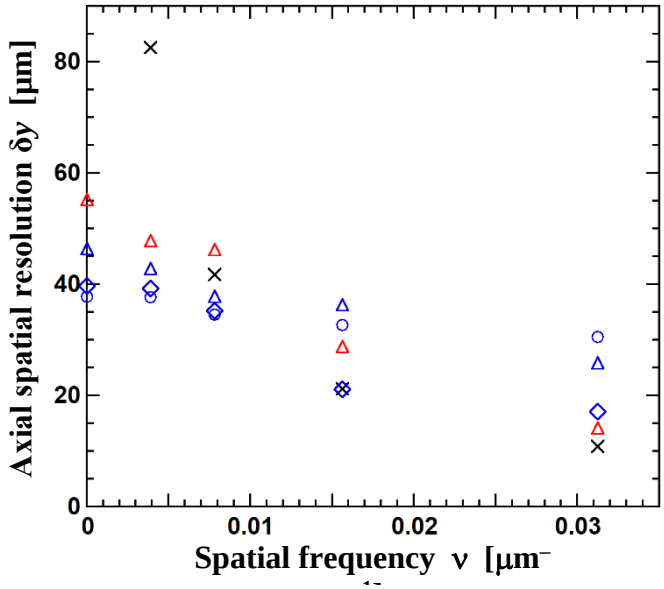

Fig. 3 Experimental estimates of axial spatial resolution δy as a function of illumination spatial frequency ν for particle radii a = 1.6 μm (*blue*) and 2.5 μm (*red symbols*) and particle volume fractions φ = 0.11% (◇), 0.2% (△) and 0.35% (○). The results are compared with the theoretical relationship for a "thin fluorescent film" derived by Neil *et al.* (×)

The experimental estimates are compared with the optical section thickness Δ_0 for a general structured illumination microscope (×). This thickness is the full width at half maximum (FWHM) of the Gaussian function that describes the point spread function (PSF), namely the intensity of the signal (*i.e.*, light) scattered by a "uniform" object normalized by its maximum value (at the focal plane). The expression for the PSF $S(z)$, originally derived by Neil *et al.* and extended to a double-exposure SIM system (Chasles et al. 2007), is an Airy pattern:

$$S(z) = 2\left|\frac{J_1\left\{8\pi n\nu(NA)\sin^2(\alpha/2)\kappa^2 z\,[1-\kappa(NA)\nu/2]\right\}}{8\pi n\nu(NA)\sin^2(\alpha/2)\kappa^2 z\,[1-\kappa(NA)\nu/2]}\right|^2 \equiv 2\left|\mathrm{jinc}\left\{8\pi n\nu(NA)\sin^2\left(\frac{\alpha}{2}\right)\kappa^2 z\left[1-\frac{\kappa(NA)\nu}{2}\right]\right\}\right|^2 \qquad [3]$$

Here, $J_1(\cdots)$ is a Bessel function of the first kind of order 1, n is the index of refraction of the optical medium, ν is the spatial frequency of the structured illumination, $NA = n(\sin\alpha)$ is the numerical aperture of the imaging system, α is half the angular aperture, $\kappa = 1/\lambda$ is the wavenumber of the illumination (where λ is the wavelength), and z is the defocus, or the axial distance from the focal plane (so the focal plane is at z = 0).

The results for a = 1.6 μm, φ = 0.11% (◇) and a = 2.5 μm, φ = 0.2% (◆) are in reasonable agreement with the theoretical predictions at ν = 0.01–0.035 μm^{-1}. Based on Eq. [3], Δ_0 is minimized when $\nu = \lambda/(NA) = 0.92$ μm^{-1}, but this was not achievable in these experiments because the contrast between the illumination maxima and minima was too small for ν > 0.05 μm^{-1}. Practically speaking, the axial spatial resolution of SIM is therefore optimized by using sinusoidal illumination at the maximum value of ν where the fringes are still visible (Xi 2014).

Figure 4 shows the contrast ratio *CR*, defined to be the ratio (averaged over ~100 samples) of the intensity at the center of the particle image before and after the phase shift in the structured illumination, *i.e.*, in the first and second of the raw images, for an in-focus and out-of-focus a = 1.6 μm particle at a given illumination spatial frequency. Here, out-of-focus and in-focus particle images are defined to be those eliminated or retained, by the SIM reconstruction procedure described earlier, respectively. This ratio characterizes the contrast of the structured illumination fringes; *CR* = 1 corresponds to no change in intensity, or no modulation in the illumination, between the two raw images.

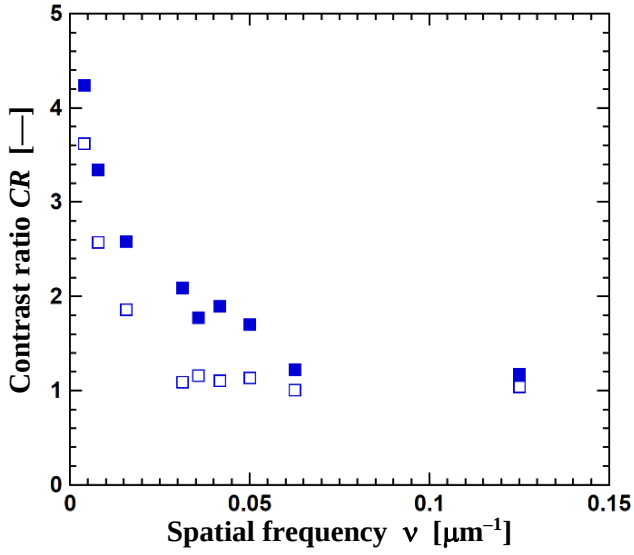

Fig. 4 Contrast ratio *CR* as a function of spatial frequency ν for in-focus (■) and out-of-focus (□) particle images

The Figure shows that *CR* decreases as ν increases, and $CR \rightarrow 1$ for $\nu > 0.05\ \mu m^{-1}$. Furthermore, because the SIM image is reconstructed from the difference between the two, the optimal spatial frequency corresponds to where the in-focus and out-of-focus particle images have the greatest difference in *CR*. In a pair of raw images, an out-of-focus particle with $CR \approx 1$ will be eliminated by the initial subtraction step of reconstruction, whereas an in-focus particle with a large *CR* will remain after subtraction, and hence in the reconstructed SIM image. The greatest difference in *CR* between the in-focus and out-of-focus particle images, of 2, occurs at $\nu = 0.031\ \mu m^{-1}$, which is also the spatial frequency that minimizes δy (Fig. 3). Hence, the rest of the results presented here are obtained at $\nu = 0.031\ \mu m^{-1}$.

Finally, δy also depends upon *a* and φ, and is hence affected by interparticle scattering. Unlike most SIM applications, the illuminated object here is a field of discrete homogenous scatterers (*i.e.*, spherical particles) whose dimensions are comparable, in order of magnitude, to the wavelength of the illumination (Bohren and Huffman 2008). The resultant Mie scattering is a function of particle size and concentration, which is known in SIM as "object dependency" (Chakrova et al. 2016).

To characterize the object dependency of SIM PTV, consider the scattering area of particles suspended in a given volume of fluid $\forall$. For a projected scattering area for a single particle of πa^2, the total projected scattering area of particles suspended at a volume fraction of φ in this volume

$$A = \frac{3\varphi \forall}{4a} \qquad [4]$$

The two cases that are in reasonable agreement with the theory given by Eq. [3] in Figure 3 have the largest *A*. Figure 5 shows experimental estimates of δy as a function of the projected scattering area of the particles per unit fluid volume $A/\forall = 0.75\varphi/a$ (in μm^{-1}) for uniform illumination (▲) and structured at illumination spatial frequencies $\nu = 7.8\times10^{-3}\ \mu m^{-1}$ (○) and $3.1\times10^{-2}\ \mu m^{-1}$ (△). For the higher spatial frequency, the axial spatial resolution increases with $A/\forall$, suggesting that interparticle scattering degrades (*i.e.*, increases) δy at optimal (*i.e.*, large) illumination spatial frequencies, and *A* should therefore be minimized. At lower ν and for unstructured (*i.e.*, dc) illumination, however, an inverse trend is observed, and δy increases as $A/\forall$ decreases. This result suggests that the modulation of the structured illumination must be above a minimum

spatial frequency to significantly reduce the axial spatial resolution (*vs.* that for uniform illumination).

In order to characterize the axial spatial resolution of the microscope for a "uniform" object, or in the absence of discrete (particle) "scatterers", the point spread function (PSF) of the imaging system was estimated experimentally and compared with the PSF predicted by Eq. [3] (Meng et al. 2017). In brief, a few a = 2.4 μm particles were immobilized in a transparent polymer (Carbopol 940) gel. A single particle in the gel was illuminated with both structured and uniform illumination and translated through the focal plane of the imaging system over defocus values -15 μm ≤ z ≤ 15 μm. The recorded particle image is the convolution of the PSF and the intensity distribution of the particle in object space, so I, the intensity at the center of the particle image, normalized to unity, as a function of z is an estimate of the PSF.

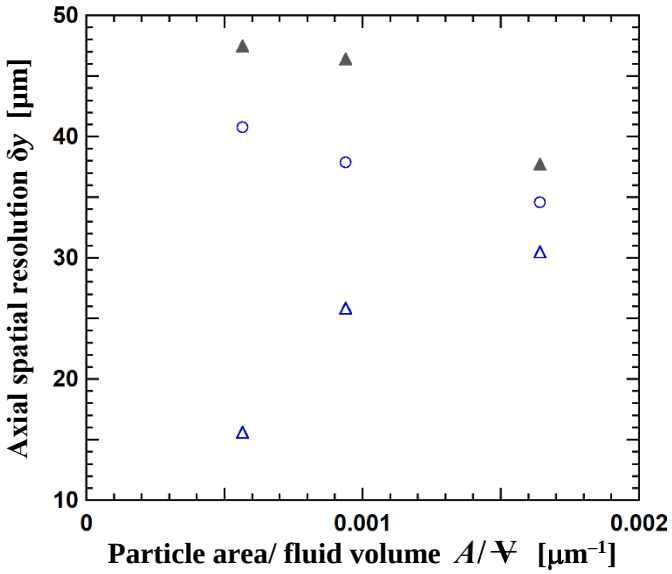

Fig. 5 Experimental estimates of axial spatial resolution δy as a function of particle area per unit fluid volume $A/\mathcal{V}$ for uniform illumination (▲) and structured illumination at ν = 0.0078 μm^{-1} (○) and 0.031 μm^{-1} (△)

Figure 6 shows experimental data for $I(z)$ for both structured and uniform illumination. Since the Airy pattern intensity given by Eq. [3] is well-approximated by a Gaussian function (Zhang et al. 2007). Gaussian functions are curve-fit to these data (*lines*), and the FWHM of the Gaussian is taken to be δy. As expected, the PSF for structured illumination is narrower than that for the uniform illumination PSF, with FWHM, or δy, of 13.5 μm and 15.2 μm, respectively. Furthermore, the value for structured illumination, namely δy = 13.5 μm, is in excellent agreement with the axial spatial resolution predicted by Eq. [3] of 13.47 μm. This calibration confirms that the characteristics of the illumination and imaging system are consistent with previous SIM systems.

In its original implementation by Neil et al., SIM used three raw images for reconstruction, as opposed to two for double-exposure SIM. To determine the effect of the number of raw images on the axial resolution of SIM PTV, SIM images were reconstructed from three (*vs.* two) raw images of Poiseuille flow using the setup shown in Fig. 1 at $\nu = 0.0325$ μm^{-1} (*i.e.*, the value that minimizes δy based upon Fig. 3) with a phase shift of $2\pi/3$ between successive images. Velocity data were obtained at the channel centerline ($y = 0$) using $a = 1.6$ μm particles at $\varphi = 0.2\%$ these results were compared with those obtained for double-exposure SIM under otherwise identical conditions. Based upon the standard deviations in the velocity data, $\delta y = 21.4$ μm for "classic" three-image SIM, *vs.* 19 μm for double-exposure SIM. This suggests that increasing the number of raw images used to reconstruct a SIM image does not improve the axial spatial resolution, at least under the conditions studied here.

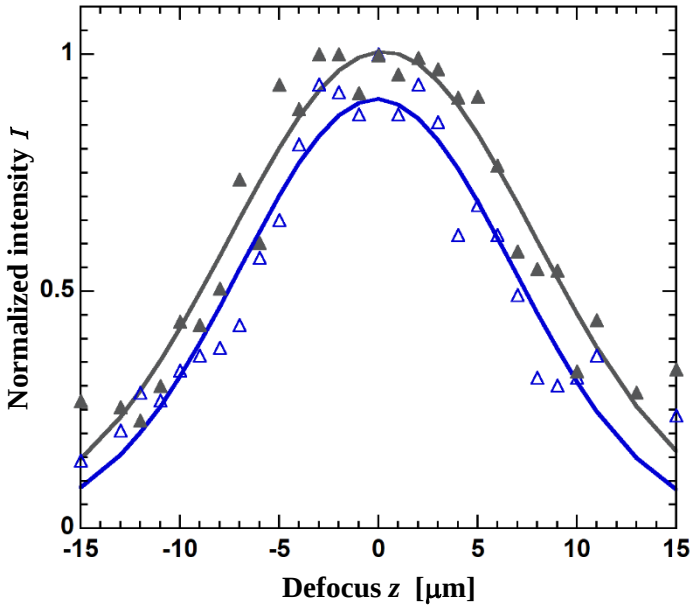

Fig. 6 Normalized intensity I as a function of defocus z of the light scattered by a single particle with structured (△) and uniform illumination (▲). The solid lines represent Gaussian curve-fits to the data

Temporal Resolution

Based on these results, SIM improves the axial spatial resolution for flows compared with uniform, or unstructured, illumination. This improvement in spatial resolution comes, however, at the expense of temporal resolution, since two raw images are required for SIM, *vs.* a single image for uniform illumination. Here, we consider two estimates of the temporal resolution of SIM PTV: 1) the time required to obtain a pair of raw images (with structured illumination) T_p; and 2) the total

time required to obtain enough velocity samples at a given location to obtain a statistically converged mean velocity T_v.

For the first estimate of temporal resolution, $T_p = \Delta t + T + 2\tau =$ 306 ms (*cf.* Fig. 1*c*) in these experiments. This value of T_p is, however, limited by the characteristics of the intensified CCD camera used here. The scientific CMOS cameras commonly used in particle velocimetry can obtain images at a few hundred Hz, and high-speed CMOS cameras have frame rates of at least 20 kHz. For a CMOS camera acquiring images at 20 kHz, a pair of reconstructed SIM images required to obtain particle velocimetry estimates can therefore be obtained within $T_p \leq 0.2$ ms. Note that commercially available DMDs can shift the phase of the structured illumination at rates as great as 30 kHz, well above the frame rates of the cameras quoted here.

Particle velocities estimated from a single image pair are, however, insufficient to obtain an accurate estimate of the velocity field because: 1) there are usually significant variations in the velocities over δy; and 2) a single image pair gives relatively few particle velocities given the low particle seeding densities typical of PTV. Velocity fields are usually therefore estimated from the average of particle velocities obtained from many image pairs; in μPIV, cross-correlation averaging over as many as $O(10^4)$ pairs is used to improve the SNR of the results.

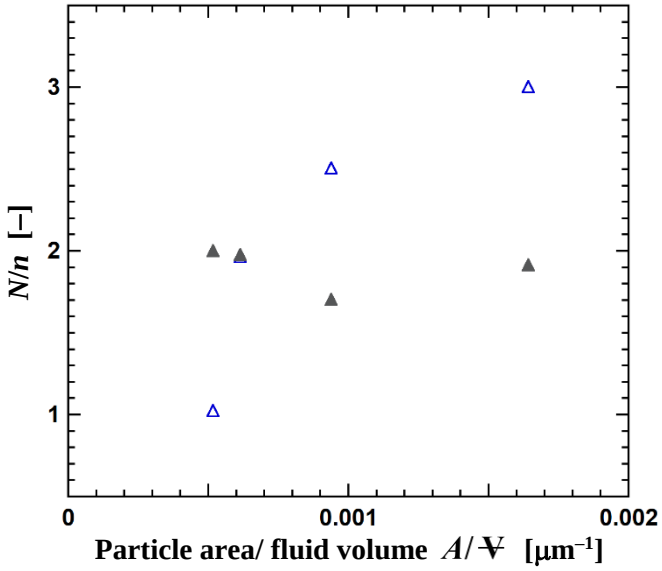

Fig. 7 The ratio N/n *vs.* the projected scattering area of the particles per unit fluid $A/\forall$ with structured (△) and uniform illumination (▲)

The time required to obtain a statistically converged mean velocity T_v, defined here to be the time required for the mean velocity to vary by less than 1%, was also estimated from the SIM results and compared to that for the results obtained with uniform illumination. This type of temporal resolution is affected by the average number of particles detected in a velocimetry image pair n and the total number of samples required to achieve statistical convergence N at a given spatial location. Hence, the ratio N/n, rounded up to the nearest integer, is the total number of image pairs required for statistical convergence of the velocity, and $T_v = (N/n)T_p$.

To determine N and n, particle images and velocities are determined from, and averaged over, a set of 10 randomly chosen pairs of reconstructed structured illumination images at $y/H = 0$ for all Re studied for a given a and φ. For the uniformly illuminated images, each image "pair" consists instead of the 1st and 3rd images in a sequence of 4 images to ensure that the time interval within the pair is comparable for both structured and uniform illumination. Hence N is determined from an average over the image area and time, and the average velocity varies by less than 1% within 10 image pairs in all cases. N and n were determined from several (3-14) sets of 10 image pairs, and N/n was found to vary by less than 15%.

Figure 7 therefore shows the average N/n as a function of the projected scattering area of the particles per unit fluid volume $A/\forall$ (*cf.* Eq. [3]) for both structured (△) and "unstructured" uniform (▲) illumination. The ratio N/n, and hence the temporal resolution T_v, increases with $A/\forall$. This suggests that the temporal resolution, like the axial spatial resolution, is degraded by interparticle scattering. Minimizing the scattering area, A therefore optimizes (*i.e.*, minimizes) this temporal resolution. Interparticle scattering appears, however, to have a negligible effect on T_v for unstructured illumination.

These results demonstrate that structured illumination gives velocities with better (i.e., lower) temporal resolution than uniform (volume) illumination at lower $A/\forall$. Indeed, the number of samples required to achieve a statistically converged mean velocity N is significantly lower for structured, *vs.* uniform, illumination in all cases. For the lowest $A/\forall = 5.2\times10^{-4}$ μm^{-1}, for example, N = 26 and 300 for structured and uniform illumination, respectively. At the highest $A/\forall = 1.6\times10^{-3}$ μm^{-1}, however, $N \approx 66$ and 528 for structured and uniform illumination, respectively. The temporal resolution of the structured illumination results increases (*i.e.*, becomes worse) with $A/\forall$ because N increases more rapidly for these results—by a factor of 2.6, while N only increase by a factor of 1.8 for the uniform illumination results over the same

range of $A/\forall$. Thus, interparticle scattering has a greater impact on the number of velocity measurements required for statistical convergence for SIM PTV.

Moreover, SIM PTV consistently identifies and matches fewer particles than "standard" PTV with uniform illumination, hence increasing the number of images required for statistical convergence. For the lowest $A/\forall = 5.2\times10^{-4}$ μm^{-1}, n = 25 and 150 for structured and uniform illumination, respectively; for the highest $A/\forall = 1.6\times10^{-3}$ μm^{-1}, n = 22 and 275 for structured and uniform illumination, respectively. The smaller n for structured illumination is mostly due to two factors. First, given that the axial spatial resolution δy for structured illumination is 17 μm and that for uniform illumination is 40 μm (*cf.* Fig. 3), the volume of fluid, and hence the number of particles n for a given φ, imaged by SIM is about 60% that for uniform illumination. Second, SIM consistently matches fewer particles within a pair of reconstructed images. Although image postprocessing removes a similar fraction—between 60% and 70%—of "particle images" in both the structured and uniform illumination images, a higher fraction of the particle images in the postprocessed structured illumination images are "artifacts", and cannot be tracked (*i.e.*, matched) to a particle image in the subsequent reconstructed image. For $A/\forall = 5.2\times10^{-4}$ μm^{-1} and 1.6×10^{-3} μm^{-1}, SIM PTV can only match 30% and 11% of the particles, respectively, using the current particle tracking approach (nearest neighbors with expected displacement), while standard PTV tracks about 67% and 73% of the particles, respectively. These results suggest that particle scattering also increases artifacts (*i.e.*, noise) in the reconstructed SIM images.

4. Summary

Structured illumination microscopy particle tracking velocimetry (SIM PTV) is a way to obtain thin slices of the velocity field in microchannel flows by strongly attenuating the signal from particles outside the focal plane by using modulated (i.e., structured) illumination. The axial spatial resolution and temporal resolution of SIM PTV were quantified over a range of experimental parameters. The spatial resolution along the optical axis, corresponding to the "thickness" of the slice imaged by the technique, was improved by a factor of two (i.e., halved) to ~14 μm, compared with ~30 μm "unstructured" uniform illumination under otherwise identical conditions. These results were obtained at higher flow speeds using smaller tracer particles compared with previous work. The axial resolution of SIM PTV was optimized (i.e., minimized) at the highest modulation frequency where the contrast at a given location between the two raw images is maximum—in other words, the highest frequency where the illumination fringes are still "visible".

This gain in axial spatial resolution, however, comes at a cost. First, modulating the illumination intensity effectively reduces the object (i.e., flow) area imaged in a single "raw" image. Second, two such images are reconstructed to create a single SIM image (and regain the object area), which degrades the temporal resolution of SIM PTV. Nevertheless, these results show that SIM PTV has temporal resolution superior to "standard" PTV in certain cases. Moreover, modern CMOS cameras with frame rates exceeding 20 kHz enable temporal resolutions of O(0.1 ms).

Ultimately, the optimal axial spatial and temporal resolutions of the technique are limited by the characteristics of the tracer particles, including radius and volume fraction. The results demonstrate that the projected scattering area of the particles should be minimized to minimize spatiotemporal resolution; this observation is a direct consequence of using structured illumination to image discrete scatterers, *vs.* a continuous object.

Acknowledgements

This work was supported by the American Chemical Society Petroleum Research Fund (Grant 57789-ND9) and the Mechanical Sciences Branch of the US Army Research Office (Contract No. W911NF-17-1-0389).

References

Adrian, R. J. (2005). Twenty years of particle image velocimetry. *Experiments in fluids*, 39(2), 159-169.

Adrian, R. J., & Westerweel, J. (2011). *Particle image velocimetry* (No. 30). Cambridge university press.

Bohren, C. F., & Huffman, D. R. (2008). *Absorption and scattering of light by small particles*. John Wiley & Sons.

Chakrova, N., Rieger, B., & Stallinga, S. (2016). Deconvolution methods for structured illumination microscopy. *JOSA A*, 33(7), B12-B20.

Chan, T. F., & Vese, L. A. (2001). Active contours without edges. IEEE Transactions on image processing, 10(2), 266-277.

Chasles, Frédéric, Benoît Dubertret, and A. Claude Boccara. "Optimization and characterization of a structured illumination microscope." *Optics Express* 15.24 (2007): 16130-16140.

Gao, Y., & Chen, L. (2008). Versatile control of multiphase laminar flow for in-channel microfabrication. *Lab on a Chip*, 8(10), 1695-1699.

Grare, S., Coëtmellec, S., Allano, D., Grehan, G., Brunel, M., & Lebrun, D. (2015). Dual wavelength digital holography for 3D particle image velocimetry. *Journal of the European Optical Society-Rapid publications*, 10.

Kim, M., & Yoda, M. (2010). Dual-tracer fluorescence thermometry measurements in a heated channel. *Experiments in fluids*, 49(1), 257-266.

Klein, S. A., Moran, J. L., Frakes, D. H., & Posner, J. D. (2012). Three-dimensional three-component particle velocimetry for microscale flows using volumetric scanning. *Measurement Science and Technology*, 23(8), 085304.

Kristensson, E., & Berrocal, E. (2018). Crossed patterned structured illumination for the analysis and velocimetry of transient turbid media. *Scientific Reports*, 8(1), 1-9.

Lee, S. J., & Kim, S. (2009). Advanced particle-based velocimetry techniques for microscale flows. *Microfluidics and Nanofluidics*, 6(5), 577-588.

Li, Y., Diddens, C., Segers, T., Wijshoff, H., Versluis, M., & Lohse, D. (2020). Rayleigh–Taylor instability by segregation in an evaporating multicomponent microdroplet. *Journal of fluid mechanics*, 899.

Lukosz, W. (1966). Optical systems with resolving powers exceeding the classical limit. *JOSA*, 56(11), 1463-1471.

Meng, Yunlong, et al. "Fast two-snapshot structured illumination for temporal focusing microscopy with enhanced axial resolution." *Optics Express* 25.19 (2017): 23109-23121.

Mishra, Y. N., Kristensson, E., Koegl, M., Jönsson, J., Zigan, L., & Berrocal, E. (2017). Comparison between two-phase and one-phase SLIPI for instantaneous imaging of transient sprays. *Experiments in Fluids*, 58(9), 1-17.

Natrajan, V. K., & Christensen, K. T. (2008). Two-color laser-induced fluorescent thermometry for microfluidic systems. *Measurement Science and Technology*, 20(1), 015401.

Neil, M. A., Juškaitis, R., & Wilson, T. (1997). Method of obtaining optical sectioning by using structured light in a conventional microscope. *Optics letters*, 22(24), 1905-1907.

Otsu, N. (1979). A threshold selection method from gray-level histograms. *IEEE transactions on systems, man, and cybernetics*, 9(1), 62-66.

Raffel, M., Willert, C. E., Scarano, F., Kähler, C. J., Wereley, S. T., & Kompenhans, J. (2018). *Particle Image Velocimetry: A Practical Guide*. Springer.

Shang, L., Cheng, Y., & Zhao, Y. (2017). Emerging droplet microfluidics. *Chemical reviews*, 117(12), 7964-8040.

Shields IV, C. W., Reyes, C. D., & López, G. P. (2015). Microfluidic cell sorting: a review of the advances in the separation of cells from debulking to rare cell isolation. *Lab on a Chip*, 15(5), 1230-1249.

Sigal, Y. M., Zhou, R., & Zhuang, X. (2018). Visualizing and discovering cellular structures with super-resolution microscopy. *Science*, 361(6405), 880-887.

Spadaro, M., & Yoda, M. (2020). Structured illumination microscopy: a new way to improve the axial spatial resolution of microscale particle velocimetry. *Experiments in Fluids*, 61(6), 1-8.

Truscott, T. T., Belden, J., Ni, R., Pendlebury, J., & McEwen, B. (2017). Three-dimensional microscopic light field particle image velocimetry. *Experiments in Fluids*, 58(3), 1-14.

Xi, P. (Ed.). (2014). *Optical Nanoscopy and Novel Microscopy Techniques* (pp. 39-40). CRC Press.

Yeo, L. Y., Chang, H. C., Chan, P. P., & Friend, J. R. (2011). Microfluidic devices for bioapplications. *Small*, 7(1), 12-48.

Yoda, M. (2020). Super-resolution imaging in fluid mechanics using new illumination approaches. *Annual Review of Fluid Mechanics*, 52, 369-393.

Yoon, S. Y., & Kim, K. C. (2006). 3D particle position and 3D velocity field measurement in a microvolume via the defocusing concept. *Measurement Science and Technology*, 17(11), 2897.

Zhang, B., Zerubia, J., & Olivo-Marin, J. C. (2007). Gaussian approximations of fluorescence microscope point-spread function models. *Applied optics*, 46(10), 1819-1829.

Zhou, X., Lei, M., Dan, D., Yao, B., Qian, J., Yan, S., ... & Chen, G. (2015). Double-exposure optical sectioning structured illumination microscopy based on Hilbert transform reconstruction. *PLoS One*, 10(3), e0120892.